Nanodomain structure of $Pb[Zr_{1-x}Ti_x]O_3$ at its morphotropic phase boundary: Investigations from local to average structure

Kristin A. Schönau,[1,*] Ljubomira A. Schmitt,[1] Michael Knapp,[2] Hartmut Fuess,[1] Rüdiger-A. Eichel,[3] Hans Kungl,[4] and Michael J. Hoffmann[4]

[1]*Materials Science, Darmstadt University of Technology, D-64287 Darmstadt, Germany*

[2]*Materials Science, Darmstadt University of Technology, D-64287 Darmstadt, Germany and CELLS, P. O. Box 68, 08193 Barcelona, Spain*

[3]*Eduard-Zintl-Institute, Darmstadt University of Technology, D-64287 Darmstadt, Germany*

[4]*Institute of Ceramics in Mechanical Engineering, University of Karlsruhe, D-76131 Karlsruhe, Germany*

(Received 23 October 2006; published 31 May 2007)

In recent years, the stability field of a monoclinic phase at the morphotropic phase boundary in lead zirconate titanate, $Pb[Zr_{1-x}Ti_x]O_3$, has been under discussion. In the present study, we investigated samples in the compositional range between $0.40 \leqslant x \leqslant 0.475$ and $x=0.55$ using high-resolution synchrotron x-ray diffraction in combination with transmission electron microscopy and electron paramagnetic resonance to correlate average structure and microstructural information. It is shown that the microstructure plays a crucial role in the analysis of diffraction data. The appearance of intensity in diffraction patterns formerly linked to a monoclinic phase [B. Noheda *et al.*, Phys. Rev. B **61**, 8687 (2000)] can directly be correlated to a miniaturization of the average domain structure of the material visible in the presence of nanodomains. The internal symmetry of the nanodomains is not necessarily monoclinic due to coherence effects in diffraction and is discussed with respect to martensitic theory.

DOI: 10.1103/PhysRevB.75.184117 PACS number(s): 77.84.Dy, 61.10.Nz, 68.37.Lp, 76.30.−v

I. INTRODUCTION

The origin of the high piezoelectric response at the morphotropic phase boundary (MPB) in ferroelectric perovskite solid solutions such as lead zirconate titanate, $Pb[Zr_{1-x}Ti_x]O_3$ (PZT), which separates the rhombohedral ($R3m$) and tetragonal ($P4mm$) phase regions,[1] has been the subject of discussion for many years. So far, physical properties are interpreted as either the reaction of an assumed domain structure to the applied electric field or as changes in symmetry or phase fractions of an average structure model. No connection between the two has been drawn up to this point. A detailed interrelation of average structure information from x-ray diffraction with real structure models derived from transmission electron microscopy (TEM) and additional information on atomistic coordination using electron paramagnetic resonance (EPR) of PZT compositions at the MPB is therefore mandatory.

The discussion on the average structure of the material at its MPB is still controversial. As the space-group symmetry of the tetragonal and rhombohedral ferroelectric phases is not connected by direct group theoretical correlation, a coexistence[2] of both was assumed. The presence of both structural modifications would enhance the capability of reaction of the material to an applied external electric field[3] due to a possible combination of six polarization directions in the tetragonal phase and eight in the rhombohedral. As a possible origin for a phase coexistence, e.g., quenched-in thermal fluctuations were considered.[2] Detailed reviews can be found in Refs. 4–6.

Furthermore, the existence of an intermediate monoclinic Cm phase—a subgroup of both the tetragonal and rhombohedral symmetries—was proposed, as Noheda *et al.*[7] detected an increase in peak width of the tetragonal 101 peak in PZT 52/48 with decreasing temperature. A maximum in width was observed around 300 K, accompanied by peak splitting in high-resolution synchrotron powder-diffraction patterns recorded in flat-plate reflection geometry.[8,9] To explain the formation of this phase, a freezing-in of local disorder in atomic positions was postulated. A possible disorder of lead was derived from anisotropic atomic displacement parameters (ADPs) used in Rietveld refinement in single-phase samples near the MPB,[8,10] in the shape of flat ellipsoids perpendicular to the respective ferroelectric polarization direction (which is $[001]_C$ in the tetragonal and $[111]_C$ in the rhombohedral phase). If this thermal motion is condensated within the $(110)_C$ plane, which contains both ferroelectric displacement directions, the symmetry is reduced to Cm and forms one of the rare cases of a two-dimensional ferroelectric, in which the dipole moment can rotate in the plane containing the polar axis.[8,11] The model was underlined by the interpretation of diffuse streaks in higher-order zones of TEM diffraction images by Glazer *et al.*[6] They further stated that larger regions of this Pb disorder were stable at the MPB, resulting in a coherently diffracting monoclinic intermediate phase. However, it was not discussed how the relation between domain structure and this new phase could be.

Peak profiles of the diffraction patterns of ferroelectric materials are highly influenced, as their structure is not completely three-dimensional periodic but contains a set of altering domains (twins) with distinct polarization directions.[12] So Rietveld refinement, which is based on three-dimensionally periodic structures, can only result in a structural model, which is an idealized assumption of the structure present. All the real structure and local structure information accessible must therefore be discussed in context with structural information derived from diffraction data.

It has been reported that the domain structure causes anisotropic broadening effects of distinct *hkl* reflections, asymmetries, and diffuse intensity between the peaks in diffraction patterns, as described for $PbTiO_3$ by Boysen.[13] He attributed asymmetries and diffuse scattering to strain deforming the lattice across the domain walls in the material. Floquet *et al.*[14] described the 90° domain wall in $BaTiO_3$ as a crystallographic discontinuity, in which irregular atomic displacement and a distribution of *d* spacings over a range of 4–5 nm cause changes in the direction of the polarization vector. However, computational studies[15] on domain walls calculated the width of both 90° and 180° domain walls in $PbTiO_3$ to be in the range of one unit cell, 0.5 ± 0.05 nm. Narrow widths of 1.0 ± 0.3 nm were also detected by Stemmer *et al.*[16] in $PbTiO_3$ using a combination of high-resolution TEM and quantitative image analysis.

All groups working on x-ray data of samples close to or at the MPB encountered similar difficulties in refining the structural models due to overlapping and asymmetric peaks, anisotropic peak broadening, and diffuse scattering. Single-phase models were used[8] as well as various two-phase combinations of tetragonal, rhombohedral, and monoclinic phases.[17–19] Ragini *et al.*[17] obtained the best fit of their data by using a combination of a tetragonal and a monoclinic structure and not single-phase models as Noheda *et al.*[8,9] and Frantti *et al.*[18] The latter two additionally modeled the diffuse intensity between, e.g., the 002/200 pair, which is ascribed to a lattice distortion across domain walls, using a cubic phase similar to the work of Müller *et al.* on $PbHf_{0.4}Ti_{0.6}O_3$.[20]

As there are obvious differences between the width of domain walls derived from TEM analysis or simulations and that predicted from x-ray diffraction, a different approach to explain the peculiarities in the diffraction patterns has to be undertaken. Interference effects between the domains were successfully discussed by Khachaturanyan and co-workers[21–27] for the structure of morphotropic relaxor ceramics [lead magnesium niobate–lead titanate (PMN-PT) and lead zinc niobate–lead titanate (PZN-PT)] using martensitic theory. In Ref. 21 and 22, the authors questioned the existence of a monoclinic phase in these materials. They stated that the lattice parameters of the monoclinic phase calculated using Rietveld refinement are directly dependent on the lattice parameters of the tetragonal and cubic parent phases and are just an average over miniaturized tetragonal nanodomains, which can reach up to tens of nanometers without being able to diffract incoherently. The miniaturization of the domain structure is induced by a very low domain-wall energy. Both the miniaturization and a low domain-wall energy can enhance piezoelectric properties of the material, as domains are more easily reoriented. We will show that in morphotropic PZT, a similar variation of the domain structure is observed in the region stated to contain a monoclinic phase.

Recent calculations on stability fields in the PZT phase diagram,[28] which are to satisfy the Gibbs phase rule, again raised the question of a two-phase region of rhombohedral and tetragonal symmetries on a nanometer length scale. This, in fact, can be correlated with our observations made in samples with compositions belonging to the MPB.

II. EXPERIMENT

For the investigation of the average and local structures at the morphotropic phase boundary, a set of samples ranging across the compositional area was subjected to x-ray synchrotron powder diffraction, transmission electron microscopy, and electron paramagnetic resonance spectroscopy. The undoped samples were prepared using a mixed-oxide route[29] with Zr/Ti contents of 60/40, 57.5/42.5, 56/44, 55/45, 54/46, 52.5/47.5, and 45/55. The powders were pressed uniaxially into 12 mm pellets at 17.7 MPa, followed by cold isostatic pressing at 400 MPa. The pellets were then sintered under an oxygen atmosphere at 1225 °C for 2 h with a heating rate of 5 °C min^{-1} up to this temperature. To minimize PbO loss through sublimation, the samples were sintered in a powder bed of $PbZrO_3$ and ZrO_2.

High-resolution synchrotron x-ray powder-diffraction measurements were conducted at the beamline B2, Hasylab Hamburg, Germany. Polycrystalline pellets of a thickness of 50–70 μm were analyzed in transmission geometry using a high-resolution setup with a scintillation single counter and analyzing crystal[30] at an incident wavelength of $\lambda \sim 0.05$ nm and a step size of 0.004°. Analysis of the grain size was conducted on mechanically polished and chemically etched samples on a Zeiss DSM 962 working at 25 kV. The mean grain size was determined as 22.1 ± 1.4 μm using a linear intercept method with program LINCE 2.31D.[31]

The x-ray data were analyzed using the general structure analysis[32] program GSAS for Rietveld refinement. A two-phase model of a tetragonal *P*4*mm* phase and a monoclinic *Cm* phase (Table I) was used in accordance with the refinement of Ragini *et al.*[17] The structural model was fitted to the data using a Thompson-Cox-Hastings pseudo-Voigt profile function,[33] and for simulation of the background, a linear interpolation between fixed background points. To partly accommodate the anisotropy in the full width at half maximum (FWHM) caused by the domain structure, the profiles were additionally varied using the generalized model for anisotropic peak broadening by Stephens,[34] incorporated in GSAS. The atomic coordinates of Zr and Ti were only refined constrained at one position to stabilize the fit, although pair distribution function modeling by Egami *et al.*[35] showed that the Zr atoms tend to stay in a central position, while the Ti is shifted out of the center to accommodate the size difference between the two types of cell. Moreover, the profile parameters, histogram scale factor, isotropic ADPs, and phase fractions were refined besides the lattice parameters. The sum of phase fractions was constrained to equal 1; further constraints were put on the ADPs of one atom type for one phase. The Thompson-Cox-Hastings profile parameters without microstrain parameters were set to be equal for both phases. We abandoned the use of any anisotropic ADPs, as strong correlation effects between profile parameters and ADPs are observed. Since peak profiles are only partially corrected for real structure effects, using isotropic ADPs some U_{iso} tend to have unphysical negative values, showing up the limitations of the fit. Similar observations were made by Corker *et al.*[10] and Frantti *et al.*[36] The latter tried to overcome the problem by independently refining the Zr and Ti positions in the *Cm* phase, however, having to constrain all U_{iso} values in the *P*4*mm* to the same value.

TABLE I. Atomic positions of the phases used in Rietveld refinement for PZT 54/46.

	Tetragonal *P*4*mm*					Nanodomains (monoclinic *Cm* fit)				
Atom	*X*	*Y*	*Z*	$U_i \cdot 100$	Site symmetry	*X*	*Y*	*Z*	$U_i \cdot 100$	Site symmetry
Pb^{2+}	0.000	0.000	0.000	5.5(4)	4*MM*(001)	0.000	0.0	0.0	4.5(2)	*M*(010)
$(Zr/Ti)^{4+}$	0.500	0.500	0.505(4)	4.0(8)	4*MM*(001)	0.478(3)	0.0	0.555(2)	1.7(3)	*M*(010)
O_1^{2-}	0.500	0.500	0.010(2)	−3.3(8)	4*MM*(001)	0.481(5)	0.0	0.143(7)	0.2(6)	*M*(010)
$O_{2/3}^{2-}$	0.000	0.500	0.547(30)	−3.3(8)	*MM*2(001)	0.282(3)	0.335(3)	0.387(6)	0.2(6)	1

Samples for transmission electron microscopic examination were prepared by the standard procedure of sawing, polishing, disk cutting, dimpling, and ion milling.[37] Transmission electron microscopy was performed with a Philips CM20 SuperTwin operating at 200 kV. Domain configurations were studied using bright field imaging and selected area electron diffraction techniques. For analysis of the symmetry within single domains, information from convergent beam electron diffraction (CBED) was used.[38] A continuative and more detailed analysis of microscopic studies can be found in Ref. 37.

Additionally, EPR investigations on Fe_{Ti}^{3+} impurity centers in nominally undoped PZT samples were undertaken. The *X* band (9.4 GHz) continuous-wave (cw) EPR measurements were performed using an ESP 300E spectrometer (Bruker), equipped with a rectangular TE_{112} resonator. The magnetic field was read out with a NMR gauss meter (ER 035M, Bruker) and, as a standard field marker, polycrystalline diphenylpicrylhydrazyl with an electron *g* value of $g=2.0036$ was used for the exact determination of the resonance magnetic-field values. The paramagnetic Fe_{Ti}^{3+} center, which is always present in low abundance as an extrinsic impurity, was used as a probe for the local point symmetry at the B site.[39–42] For the discussion of the corresponding high-spin $3d^5$ Fe_{Ti}^{3+} EPR spectra $\left(S=\frac{5}{2}\right)$, which, in principle, should include tensor components up to fourth-rank,[43,44] a simplified effective spin Hamiltonian[42,41] given by

$$\mathcal{H} = g_{\mathrm{iso}}\beta_e \mathbf{B}_0 \cdot \mathbf{S} + B_2^0 O_2^0 + B_2^2 O_2^2 \qquad (1)$$

was used, in which g_{iso} is the electron *g* value, β_e the Bohr magneton, and B_0 the external field. The first term represents the electronic Zeeman interaction, and the last two terms describe the second-rank fine-structure (FS) interaction, where B_2^0 and B_2^2 are the corresponding FS parameters and O_2^0 and O_2^2 the extended Stevens spin operators.[43] Principally, EPR allows no direct assignment to either rhombohedral or monoclinic symmetry and renders a FS interaction tensor of orthorhombic symmetry $(B_2^0 \neq 0 \wedge B_2^2 \neq 0)$ for both cases. However, the existence of different orthorhombic phases may generally be determined, as multiple sites with corresponding ratios B_2^2/B_2^0 will be observed and a clear distinction from tetragonal symmetry $(B_2^0 \neq 0 \wedge B_2^2 = 0)$ is provided. Correspondingly, EPR is used here to determine the number of different sites and their relative intensities.

III. RESULTS

To understand the effects visible in the diffraction pattern of samples with composition in the morphotropic phase region, we first investigate the influence of the domain structure on the tetragonal and rhombohedral side of the MPB before we consider the area, where a monoclinic phase was observed by Noheda *et al.*[8]

A. Synchrotron x-ray diffraction and TEM: PZT of tetragonal symmetry

In x-ray powder-diffraction patterns of tetragonal PZT 45/55, anisotropic peak broadening effects and asymmetries in line shape are observed for distinct *hkl* reflections. Broadening is most pronounced in *l*-dependent reflections, while *h*-dependent reflections are sharpest. The FWHM of *h*0*h* reflections take on intermediate values. The asymmetries, partly accompanied by diffuse scattering, are dominant between reflection pairs which are split with respect to cubic symmetry (Fig. 1, topmost pattern). The Rietveld fit using a *P*4*mm* symmetry and symmetric anisotropic peak broadening[34] leads to characteristic small misfits as asymmetries cannot be adjusted. This is in agreement with reports on the effect of tetragonal domains on diffraction patterns of pure $PbTiO_3$ by Boysen.[13] TEM investigations on tetragonal PZT samples reveal a bimodal lamellar distribution of domain widths of mostly 90° domains, which is fluctuating around average values of 66 and 147 nm.[37] According to martensitic transformation theorem,[45] the domain walls should be stress-free and the domain widths in the plane of projection should be in the range detected by Schmitt *et al.*[37]

B. Synchrotron x-ray diffraction and TEM: PZT of rhombohedral symmetry

New discussions on the symmetry of samples on the Zr-rich side of the MPB arose when Ragini *et al.*[17] postulated that its crystal structure at ambient temperature was not rhombohedral but monoclinic, as in Rietveld refinement the goodness of fit using a *Cm* phase was better than for an *R*3*m* phase. They underlined their statement with the work of Corker *et al.*,[10] who considerably improved their fit on neutron powder diffraction data from samples with rhombohedral compositions of Ti up to a content of 40 mol % by using an *R*3*c* phase and anisotropic ADPs. However, CBED for our PZT 60/40 samples with the sintering temperature already as low as 1050 °C clearly report rhombohedral symmetry

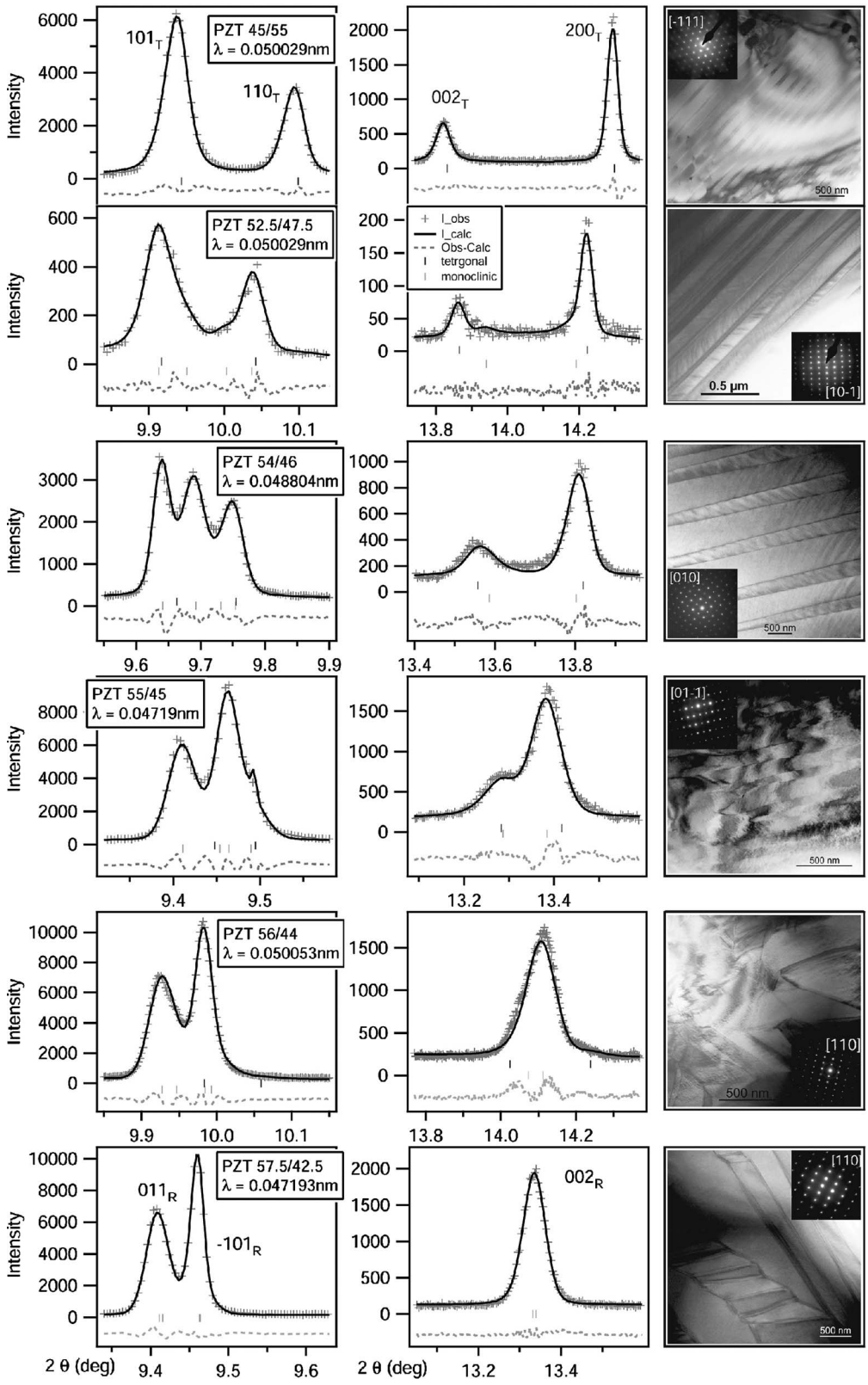

FIG. 1. High-resolution synchrotron x-ray powder diffraction and TEM imaging of PZT of varying Zr/Ti ratio. An increase in broadening is seen in changes in shape and width of the 002_T reflection between the sample PZT 45/55, 52.5/47.5, and 54/46. The asymmetry and width of the tetragonal 101_T reflection not only change but also evolve into a new peak between 101_T 110_T in sample PZT 54/46, which gains in intensity toward PZT 57.5/42.5. This rise is accompanied by a decrease in intensity of the visible 110_T reflection, which then seems to be absent or overlapped in sample PZT 56/44, and a splitting of the cubic and/or tetragonal 111 reflection. The domain structure changes from a lamellar tetragonal configuration via nanodomains to a rhombohedral herringbone structure.

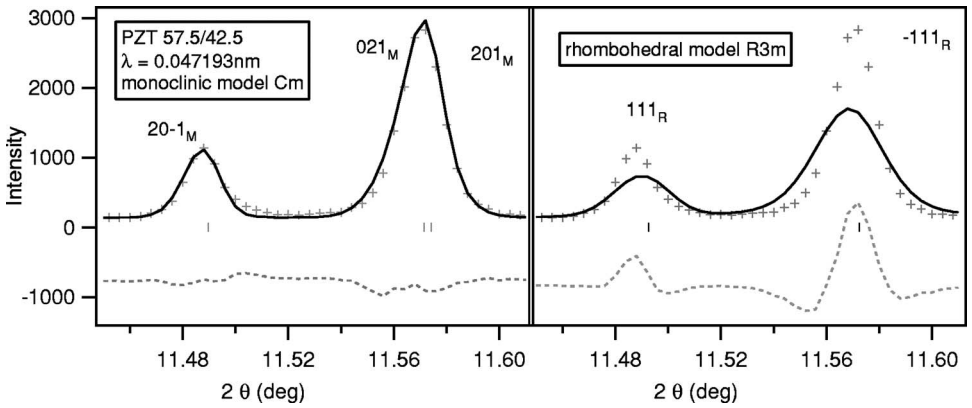

FIG. 2. Rietveld fit of PZT 57.5/42.5 using a monoclinic *Cm* cell and a rhombohedral *R*3*m* cell.

within a domain.[38] As diffraction experiments for both sintering temperatures of 1050 and 1225 °C do not show differences in features besides symmetric broadening due to grain-size effects, this result can directly be extrapolated to samples of higher sintering temperature. The difficulty of refining the structural model for high-resolution diffraction data of PZT 60/40 and PZT 57.5/42.5 using a rhombohedral *R*3*m* symmetry sheds some doubts on the existence of a monoclinic phase in PZT. Anisotropic broadening effects in diffraction patterns of these samples are very pronounced and can not be accommodated using anisotropic peak broadening parameters by Stephens[34] for a rhombohedral *R*3*m* symmetry. The deviation from an ideal rhombohedral diffraction pattern arises from the difficulty of arranging the eight possible polarization directions in the rhombohedral phase in a three-dimensional set of domains. This causes domain walls to be strained and be of predominantly wavy character, separating large rhombohedral domains of lamellar or herringbone structure.[37] In diffraction, these strain effects result in additional anisotropic broadening of diffraction peaks besides coherence effects, as clearly visible for $00l_R$ reflections. This plane coincides with a 71° domain wall.[46] The largest mismatch between a fit using an *R*3*m* symmetry and additional rhombohedral microstrain parameters and the measured data is observed in the $111_R/\bar{1}11_R$ reflection pair, for which the calculated pattern gives broader reflection widths (Fig. 2). If instead a monoclinic *Cm* phase is used in combination with anisotropic peak broadening parameters, the reduced χ^2 (goodness of fit) decreases drastically and all reflection widths and intensities are fitted correctly. The *c*/*a*-ratio of the monoclinic fit, calculated for pseudocubic axes, is around 1. It is thus demonstrated that a complex and strained domain structure alters a diffraction pattern in such a way that it may be fitted using a symmetry model, which is not supported by other techniques.

C. Synchrotron x-ray diffraction: PZT of morphotropic composition

We now investigate samples of morphotropic composition starting on the tetragonal side of the MPB. With higher Zr content, the broadening of the *l*-dependent tetragonal reflections increases. In addition, a rising distribution of *d* values reflected in peak asymmetry between—with respect to the cubic phase—split reflections is observed (Fig. 1). At the same time, the tetragonal *c*/*a*-ratio of the samples decreases (Fig. 3). A gain in intensity between 101_T and 011_T evolves into a new peak alike $\bar{1}01_R$. However, the presence of a rhombohedral phase cannot be certified, as no unoverlapped rhombohedral 002_R peak is observable in PZT 54/46. PZT 55/45 represents an intermediate between PZT 54/46 with higher tetragonal *c*/*a*-ratio and PZT 56/44 with overlapping broad peaks and a very small tetragonal *c*/*a*-ratio. The peak width of the {002} reflection derived from single peak fits has a maximum at this composition (Fig. 3).

With the strong increase in anisotropic peak broadening and asymmetry with respect to a tetragonal symmetry, it is not possible to apply a standard tetragonal Rietveld fit to samples on the tetragonal side of the MPB. The question on coexistence of a second phase arises. All possible one-, two-, and three-phase symmetry combinations of *P*4*mm*, *Cm*, and *R*3*m* were tested. The best fit was achieved using a combination of the tetragonal and monoclinic phases. This way, anisotropy and especially the asymmetry of reflections were accounted for, as the peak positions of the *Cm* monoclinic phase lie directly underneath the asymmetric tails of tetragonal reflections, visible, e.g., in the monoclinic $002_M/220_M$ reflections with relation to the tetragonal $002_T/200_T$ pair (Fig. 1, PZT 52.5/47.5 or PZT 54/46). Moreover, the additional reflection between 101_T and 110_T in PZT 54/46, which cannot be attributed to the tetragonal phase, and the splitting of the 111_T reflection are accommodated with the addition of a *Cm* phase. A full pattern of PZT 55/45 is depicted in Fig. 4. This is in agreement with the refinement of Ragini *et al.*[17] A decrease in the *c*/*a*-ratio was calculated in pseudocubic axes from both the tetragonal and monoclinic fits (Figs. 3 and 5) with increasing Zr content. The tetragonal phase fraction directly goes along with its *c*/*a*-ratio and is absent for samples PZT 57.5/42.5 and PZT 60/40 on the rhombohedral side of the MPB.

These fits can imply that an additional monoclinic phase is present at the MPB as proposed in literature,[9] with a gradual changeover in phase content from tetragonal to monoclinic with increasing Zr content. However, we have to bear in mind various observations: there are no independent monoclinic reflections in the patterns which are not linked to either asymmetries of tetragonal reflections or diffuse scattering between those or to the reflection, which in samples with higher Zr content will be assigned to a rhombohedral

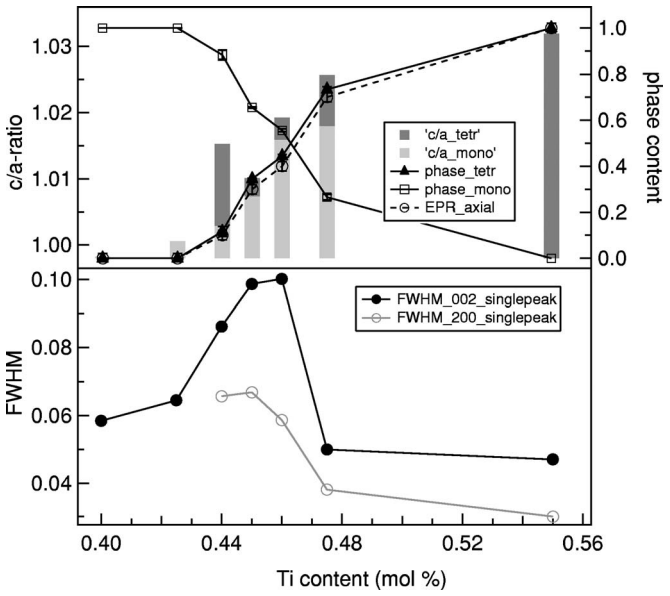

FIG. 3. Phase fractions and c/a-ratio derived from two-phase Rietveld refinement of high-resolution synchrotron powder-diffraction data (for data see Table II). Peak width from single peak fits is largest at the MPB where there is a crossover in phase fractions going along with a decrease in c/a-ratios. Phase fraction detected by XRD are directly comparable to the content of local tetragonal distortion gained by EPR analysis. At the crossover point, the peak width of the 002 reflection derived from single peak fits is at its maximum.

101_R reflection. Furthermore, by using Rietveld refinement, the features of the diffraction pattern caused by the domain structure of the material are not fully modeled, as so far no profile functions are available. Even pure rhombohedral compositions are fitted better using a monoclinic symmetry model. Whether the improved fit including a monoclinic phase is due to interference effects as assumed by Jin *et al.*[22] for PMN-PT or to monoclinic symmetry cannot be decided at this point. For further interpretation, information on the domain structure from TEM and, additionally, EPR analysis are necessary.

D. TEM: PZT of morphotropic composition

TEM studies across the MPB and for PZT 45/55 and PZT 60/40 help to clarify the picture. They are described in more detail in the work of Schmitt *et al.*[37] Drastic changes in domain configuration and size with composition are observed. The typical domain structure present on the tetragonal side (topmost TEM image in Fig. 1) miniaturizes with increasing Zr content up to PZT 55/45. First, very small domains develop within the tetragonal microdomains, which we will define as nanodomains. Their lateral size strongly varies with composition between 3 nm in samples close to the tetragonal and rhombohedral phase fields and a maximum of 30 nm in PZT 54/46.[37] Within the larger nanodomains in PZT 54/46, another smaller set of subdomains is present,[47] which makes the determination of symmetry within a single nanodomain using CBED challenging due to experimental restrictions.[38] On the tetragonal side of the MPB within the plane of projection, nanodomains predominantly take on an angle of ~45° to the domain wall of the lamellar 90° microdomains. In the TEM bright field image of PZT 54/46 in Fig. 1, the (101) microdomain walls are seen edge on with respect to the tetragonal [010] zone axis, while the nanodomains show a diffraction contrast pattern of fringes. The diminishing c/a-ratio of the tetragonal phase with decreasing Ti content is accompanied by an increase in nanodomain content and width. The orientation of the nanodomains varies locally with respect to the domain walls of microdomains in PZT 55/45 up to a perpendicular arrangement in the plane of projection. Furthermore, irregular microdomain walls with predominantly wavy character are observed for compositions between PZT 55/45 and PZT 60/40,[37] involving large internal stresses.[48] At a composition of PZT 56/44, the nanodomain width decreases again and they start to coexist with wedge-shaped microdomains. However, synchrotron data still show a percentage of 11% tetragonal phase and a very broad 200_T peak for this composition. This indicates that the sample, on average, still contains areas consisting of tetragonal microdomains. In samples with a higher Zr content, the nanodomains become smaller in width, until just microdomains are present.

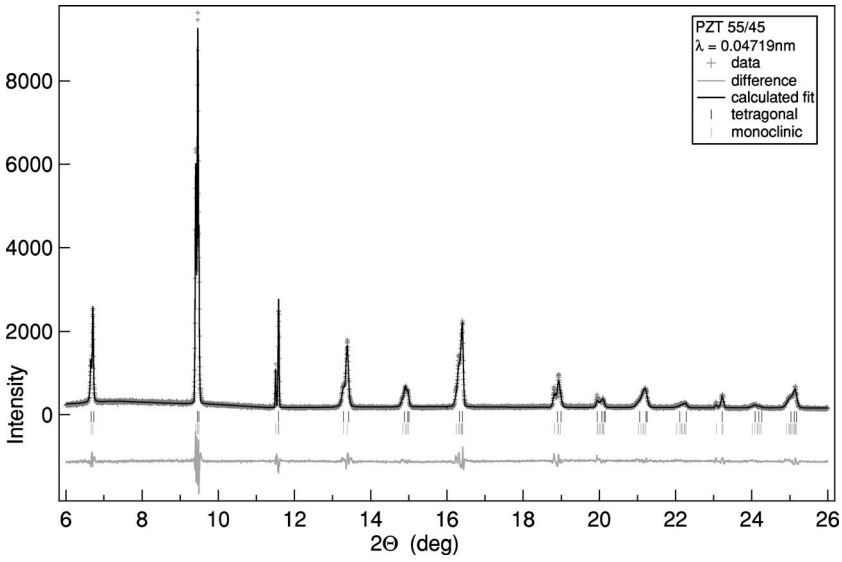

FIG. 4. High-resolution synchrotron x-ray powder diffraction of PZT 55/45. Rietveld refinement using tetragonal $P4mm$ and monoclinic Cm phases is able to model both the splitting in $\{111\}_c$ and in $\{002\}_c$ better than using single-phase fits.

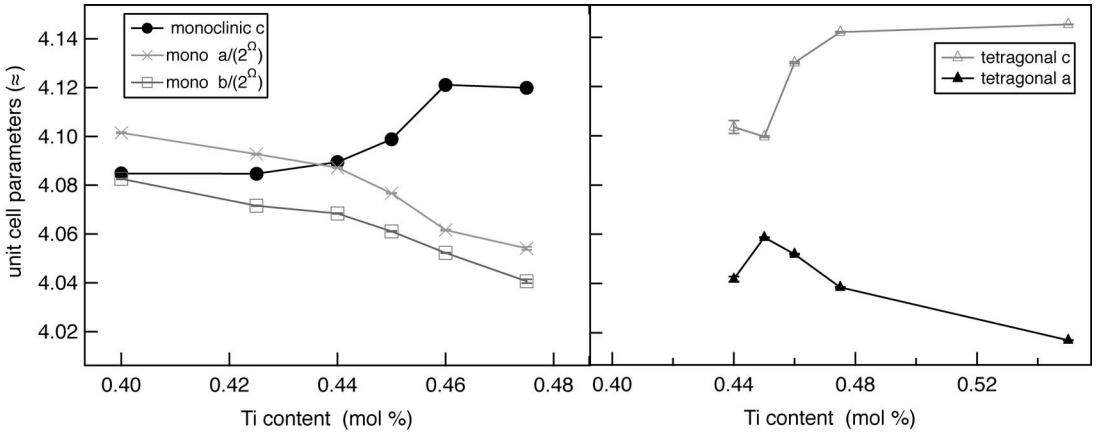

FIG. 5. Lattice parameters derived from two-phase Rietveld refinement of high-resolution synchrotron powder-diffraction data. At Ti contents lower than 0.44 mol %, the monoclinic lattice parameters, recalculated to tetragonal axes, are almost equal.

E. EPR

The obtained ambient temperature *X*-band EPR spectra for varying Zr/Ti ratios are depicted in Fig. 6. Principally, the analysis of the local structure in PZT compounds via the $Fe^{3+}_{Zr,Ti}$ paramagnetic probe is complicated by the existence of charge-compensating oxygen vacancies ($V_O^{\cdot\cdot}$) in the first coordination sphere of the Fe^{3+} centers.[39,41] These lattice vacancies induce an additional orthorhombic distortion to the local crystal field already in the global tetragonal phase.[49] However, in good approximation, this additional distortion may be treated as a constant offset.[50] Taking the spectrum for a composition of PZT 45/55 with tetragonal symmetry as constituent reference spectrum, this constant "orthorhombic offset" may be determined to an axial-to-orthorhombicity ratio of 0.27. By determining the axial-to-orthorhombicity ratio for different Zr/Ti ratios through numerical spectrum simulation, the effective phase ratio may be obtained by "subtracting" this extra offset from all other spectra. Concerning the numerical spectrum simulation, the exact values for B_2^0 are not yet determined for the Fe^{3+}_{Ti} impurity center in PZT solid solutions. As these parameters are not accessible from the low-frequency condition-type EPR spectra, lower and upper bounds for B_2^0 are defined by the values obtained from the pure phases Fe^{3+}_{Ti}:$PbTiO_3$ (Ref. 42) and Fe^{3+}_{Zr}:$PbZrO_3$,[41] respectively. This proceeding is justified, because in the low-frequency regime, established at *X*-band microwave frequencies, even large variations in the FS interaction do only influence the positions of the resonance lines in fourth order, as long as the condition $B_2^0 \gg \hbar\omega$ is fulfilled.[51] On the contrary, *X*-band EPR is very sensitive to subtle changes in the local symmetry via variations in the line intensities or variations in the size of B_2^2, for which reason it is well suited for investigating the local structure. The corresponding phase contents as a function of composition are shown in Fig. 3 and go along with the phase fraction determined by x-ray diffraction (XRD). As a further result, the width of the MPB may roughly be determined as ranging from PZT 52/48 to 56/44 for ambient temperature.

IV. DISCUSSION

The results presented above strongly indicate that the domain structure plays the leading role in the interpretation of diffraction data from PZT.

Already for single-phase tetragonal material, the classical interpretation of diffraction data using a wide crystallographic discontinuity[14] or strain fields across domain walls[13] is not supported by computational studies[15] on the width of domain walls and recent TEM investigations.[16] Both studies determined the width of a domain wall to be one or two unit cells. This is in correspondence with martensitic theory, which requests the domain wall to be an invariant plane and therefore strain-free. An origin for the observed anisotropic broadening can be the variation in domain size and width, detected in TEM investigations.[37] An indication for this is that the broadening can mostly be modeled using anisotropic peak broadening parameters, implying that the distribution of size and, possibly, strain is quite homogeneous within the sample. Strain at four-domain junctions in tetragonal doped PZT was determined by MacLaren *et al.*,[52] so strain effects cannot be ruled out. As the angle between 90° domains slightly deviates from 90°, coherence effects between stacked domains govern the asymmetries between split reflections. These changes in peak shape remain unaccounted using Rietveld.

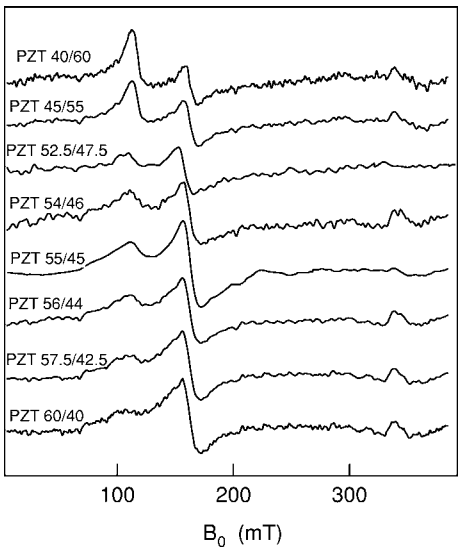

FIG. 6. *X*-band EPR spectra of PZT compounds with varying Zr/Ti ratio.

TABLE II. Composition-dependent lattice parameters, phase fractions, and c/a-ratio.

	Tetragonal *P*4*mm*				Nanodomains (monoclinic *Cm* fit)						EPR
Zr/Ti	a_T (Å)	c_T (Å)	fraction	$(c/a)_T$	a_M (Å)	b_M (Å)	c_M (Å)	β (deg)	Fraction	$(c/a)_M$	EPR(axial)
60/40			0		5.798	5.764	4.091	90.430	1	1.001	0
57.5/42.5			0		5.788	5.758	4.085	90.446	1	1.001	0
56/44	4.042	4.103	0.116	1.015	5.780	5.754	4.090	90.466	0.884	1.003	0.10(2)
55/45	4.059	4.099	0.345	1.010	5.765	5.743	4.098	90.459	0.655	1.007	0.30(2)
54/46	4.052	4.130	0.444	1.019	5.744	5.730	4.121	90.431	0.556	1.016	0.40(2)
52.5/47.5	4.039	4.142	0.734	1.026	5.733	5.714	4.120	90.302	0.226	1.018	0.70(2)
45/55	4.017	4.145	1	1.032					0		1

In samples of the rhombohedral side of the MPB, domain walls are strained and anisotropic peak broadening does not follow space-group symmetry restrictions for an *R*3*m* phase. Corker *et al.*[10] improved their fits of data from rhombohedral samples by the introduction of anisotropic ADPs, which were interpreted as local lead disorder and served as a basis for the model of a monoclinic phase by Noheda *et al.*[9] and Glazer *et al.*[6] As we have shown above, the refinement of these data is influenced by the strained domain structure, and the symmetry applied to get the best goodness of fit in Rietveld refinement is not necessarily the intrinsic structure of the material. If a profile is not matched correctly, a refinement of anisotropic thermal parameters can partly compensate this mismatch, and it is therefore difficult to determine the real origin of the effect. The question remains whether the same anisotropic ADPs, as reported by Corker *et al.*, were still observable if an implementation of the effects of the strained domain walls and coherence between the domains is achieved. Therefore, simulation work using DIFFAX+ (Ref. 53) to apply possible stacking models is in progress.

In view of the results on single-phase material, we need to reconsider the view of the structure at the MPB discussed in literature. The presence of a single monoclinic phase, as postulated by Glazer *et al.*,[6] which is to form large areas that diffract incoherently, should manifest itself in the electron microscope. However, besides tetragonal or rhombohedral microdomains, whose symmetry can be verified using CBED,[38] only nanodomains are observed. The appearance of the additional intensity between the 101_T and 110_T reflections in PZT 54/46, so far attributed to a monoclinic phase, may well be a result of coherence effects between nanodomain structures. Then, no information on the internal symmetry of the nanodomains can directly be gained from diffraction, as tetragonal, monoclinic, and rhombohedral nanodomains all show up as a monoclinic phase in the diffraction pattern.[26]

Based on martensitic theory, the internal structure of the nanodomains can be estimated.[22] If the internal symmetry is unchanged with respect to that of the tetragonal parent phase, the "adaptive" monoclinic phase will have a *Pm* symmetry, as in PMN-PT. However, if the adaptive lattice parameters of the *a* and *b* axes are related to those of the parent tetragonal phase via a $\sqrt{2}$ dependence, the internal symmetry of the nanodomains is likely to be rhombohedral.[21] The latter dependence would result in the observation of a monoclinic *Cm* phase, as in the area of the MPB in PZT.

By the application of a two-phase Rietveld fit of a tetragonal *P*4*mm* phase and monoclinic *Cm* phase, the fraction of tetragonal microdomains and of nanodomains can be quantified. The reduction in phase fraction of the tetragonal phase with increasing Zr content goes along with its reduction in c/a-ratio and is therefore connected to a decrease in domain-wall energy—an observation supporting the idea of a miniaturization of the domain structure in systems with low domain-wall energy.[21] The local symmetry environment changes equivalently, as described in Sec. III E.

The monoclinic cell parameters change in the same way as the tetragonal ones, decreasing in c/a-ratio (scaled to pseudocubic axes) and shifting toward rhombohedral axes of equal length (Figs. 3 and 5). If the monoclinic c/a-ratio is about 1, the content of tetragonal microdomains besides nanodomains is very low or has vanished. Considering the information obtained from Rietveld refinement of rhombohedral material, we can conclude that for a Zr content of 0.56 mol % and higher, mainly rhombohedral microdomains are present, possibly still accompanied by a small number of nanodomains.

Supporting the model applied to diffraction data, EPR measurements demonstrate for all samples of morphotropic composition a coexistence of one phase with local tetragonal symmetry environment and one phase with lower local symmetry (rhombohedral, orthorhombic, or monoclinic). While the transition between the tetragonal and this second site symmetry is clearly visible in the EPR spectra, no further change is detectable up to PZT 60/40, which is clearly shown to be rhombohedral in TEM experiments.[38] A change from monoclinic to rhombohedral or a coexistence of these two phases would result in additional resonance lines, as a different structural phase manifests in a varying B_2^2/B_2^0 ratio. This was not observed within the obtained spectral resolution. As EPR is a local probe, which is only sensitive to the coordination sphere around $Fe^{3+}_{Zr,Ti}$ centers, it could be argued that as iron in a tetragonal environment is always linked to an oxygen vacancy,[39] this atom stabilizes one type of surrounding and does not represent the average structure within the material. As in our samples iron is only present in traces, the possibility of clustering and the stabilization of local symmetry areas different to that of Zr or Ti can be ruled out.

To complete our discussion, computational simulations on phases and structures at the MPB based on first principles[54] and density-functional theory[55] have to be considered. These methods rely on a limited size of supercell, and an implemented structure relaxation may produce an energy balance different from stability fields caused by domains or micromechanical strains. Domains are electrostatically different from a relaxed lattice, while, e.g., strained domain walls in the rhombohedral phase change elastic energy balances. Monte Carlo simulations in progress by Bhattacharya and co-workers [56] take electrostatic long-range interactions between ferroelectric dipoles into account. These calculations demonstrate that even in the area of the MPB, a combination between rhombohedral and tetragonal nanodomains can be stable, while in the tetragonal and rhombohedral phases, microdomain states are stable. Recent calculations by Rossetti *et al.*,[28] using a low-order Landau expansion satisfying the Gibbs phase rule, have shown that, in the narrow range of the MPB, the thermodynamic stability of a coexisting phase field of rhombohedral and tetragonal symmetries expands with decreasing temperature, and that phase coexistence is likely to occur on a nanoscale, e.g., as nanodomains.

To obtain a more detailed insight on energy balances of the different phases, one should require information on variations in domain-wall energy of the material, which at the moment are not accessible. Only assumptions in correlation with the tetragonal distortion of the material can be made. Calculations using Landau-Ginzburg-Devonshire theory by Budimir *et al.*[57] predict that the Gibbs free-energy profile of the tetragonal phase is flattened for compositions close to the MPB. A very detailed extended discussion on this topic can be found in the work of Bell.[58] His line of argumentation is consistent with our model on nanodomain structures. If a local ordering of *B* cations appears, this can lead to the stabilization of nanostructures, which are averaged up to a monoclinic phase in diffraction.

V. CONCLUSION

Only a combination of average and local structure analyses can give a full picture of samples dominated by real structure effects. We showed that the previously reported observation of a monoclinic phase in PZT only using XRD (Ref. 8) is due to a nanodomain structure in the MPB region, and x-ray diffraction patterns are strongly influenced by the miniaturization of the average domain structure observed in TEM experiments. The amounts of nanodomains present in the structure besides tetragonal microdomains can be estimated using tetragonal and monoclinic Rietveld fits. Taking into account martensitic theory, it can be concluded that the nanodomains present at the MPB are likely to be of rhombohedral internal symmetry. However, it also has to be stated that a detailed investigation of the internal structure of the nanodomains is not accessible with standard methods. A possible outlook is the application of microdiffraction techniques.

The high piezoelectric response of PZT at its MPB was, so far, explained by a rotation of the polarization direction between tetragonal and rhombohedral symmetries.[59] With nanodomains present in the area of the MPB, a gradual rotation of the overall polarization can be achieved as well by reorientation of small nanostructures with high domain-wall mobility, similar to PMN-PT.[22] The small domains are able to react with more flexibility to the applied electric field due to smaller domain-wall energy and can assemble into larger domain structures under electric field. More insight into this behavior can be retrieved using *in situ* electric-field x-ray diffraction, which will be presented elsewhere. Therefore, nanodomain structures, previously interpreted as a monoclinic phase, may help in understanding the macroscopic properties of PZT compounds without necessarily introducing a monoclinic structure in the area.

ACKNOWLEDGMENTS

The authors would like to thank Tsutomu Mori for the excellent introduction into martensitic theory. This research has been financially supported by the German Research Society (DFG) center of excellence 595 *Electrical Fatigue in Functional Materials* and would not have been possible without the help and support of Roland Schierholz, Ralf Theissmann, Ulrike Kunz, and Gerhard Miehe. Furthermore, the authors are very grateful for intensive and helpful discussions with Beatriz Noheda, Matteo Leoni, and Doru C. Lupascu. The authors would like to thank Kaushik Bhattacharya for giving an insight on the results of the Monte Carlo simulation work in progress.

*Corresponding author. FAX: +49-6151-166377. Email address: schoenau@matgeo.tu-darmstadt.de

[1] B. Jaffe, W. R. Cook, and H. Jaffe, *Piezoelectric Ceramics* (Academic, London, 1971).
[2] W. Cao and L. E. Cross, Phys. Rev. B **47**, 4825 (1993).
[3] M. J. Hoffmann, M. Hammer, A. Endriss, and D. C. Lupascu, Acta Mater. **49**, 1301 (2001).
[4] B. Noheda, Curr. Opin. Solid State Mater. Sci. **6**, 27 (2002).
[5] B. Noheda and D. E. Cox, Phase Transitions **79**, 5 (2006).
[6] A. M. Glazer, P. A. Thomas, K. Z. Baba-Kishi, G. K. H. Pang, and C. W. Tai, Phys. Rev. B **70**, 184123 (2004).
[7] B. Noheda, D. E. Cox, G. Shirane, J. A. Gonzalo, L. E. Cross, and S.-E. Park, Appl. Phys. Lett. **74**, 2059 (1999).
[8] B. Noheda, J. A. Gonzalo, L. E. Cross, R. Guo, S.-E. Park, D. E. Cox, and G. Shirane, Phys. Rev. B **61**, 8687 (2000).
[9] B. Noheda, D. E. Cox, G. Shirane, R. Guo, B. Jones, and L. E. Cross, Phys. Rev. B **63**, 014103 (2000).
[10] D. L. Corker, A. M. Glazer, R. W. Whatmore, A. Stallard, and F. Fauth, J. Phys.: Condens. Matter **10**, 6251 (1998).
[11] S. C. Abrahams and E. T. Keve, Ferroelectrics **2**, 129 (1971).
[12] G. Arlt, J. Mater. Sci. **25**, 2655 (1990).
[13] H. Boysen, Z. Kristallogr. **220**, 726 (2005).

[14] N. Floquet, C. M. Valot, M. T. Mesnier, J. C. Niepce, L. Normand, and A. Thorel, J. Phys. III **7**, 1105 (1997).
[15] B. Meyer and D. Vanderbilt, Phys. Rev. B **65**, 104111 (2002).
[16] S. Stemmer, S. K. Streiffer, F. Ernst, and M. Rühle, Philos. Mag. A **71**, 713 (1995).
[17] Ragini, R. Ranjan, S. K. Mishra, and D. Pandey, J. Appl. Phys. **92**, 3266 (2002).
[18] J. Frantti, S. Eriksson, S. Hull, V. Lantto, H. Rundlöf, and M. Kakihana, J. Phys.: Condens. Matter **15**, 6031 (2003).
[19] J. Frantti, S. Ivanov, S. Eriksson, H. Rundlöf, V. Lantto, J. Lappalainen, and M. Kakihana, Phys. Rev. B **66**, 064108 (2002).
[20] Ch. Müller, J.-L. Baudour, V. Madigou, F. Bouree, J.-M. Kiat, C. Favotto, and M. Roubin, Acta Crystallogr., Sect. B: Struct. Sci. **B55**, 8 (1999).
[21] Y. M. Jin, Y. U. Wang, A. G. Khachaturyan, J. F. Li, and D. Viehland, J. Appl. Phys. **94**, 3629 (2003).
[22] Y. M. Jin, Y. U. Wang, A. G. Khachaturyan, J. F. Li, and D. Viehland, Phys. Rev. Lett. **91**, 197601 (2003).
[23] D. Viehland, J. Appl. Phys. **88**, 4794 (2000).
[24] S. M. Gupta, Y. M. Jin, and D. Viehland, J. Am. Ceram. Soc. **81**, 557 (1998).
[25] F. Bai, J. Li, and D. Viehland, J. Appl. Phys. **97**, 054103 (2005).
[26] Yu. U. Wang, Phys. Rev. B **73**, 014113 (2006).
[27] D. Viehland, J. F. Li, and E. V. Colla, J. Appl. Phys. **96**, 3379 (2004).
[28] G. A. Rossetti, Jr., W. Zhang, and A. G. Khachaturyan, Appl. Phys. Lett. **88**, 072912 (2006).
[29] M. Hammer and M. J. Hoffmann, J. Am. Ceram. Soc. **81**, 3277 (1998).
[30] M. Knapp, C. Baehtz, H. Ehrenberg, and H. Fuess, J. Synchrotron Radiat. **11**, 328 (2004).
[31] S. L. D. Lucato, LINCE 2.31D, TU Darmstadt, FB Materialwissenschaften, FG Nichtmetallisch-Anorganische-Werkstoffe.
[32] A. C. Larson and R. B. von Dreele, Los Alamos National Laboratory Report No. LAUR 86, 1994 (unpublished).
[33] P. Thompson, D. E. Cox, and J. B. Hastings, J. Appl. Crystallogr. **20**, 79 (1987).
[34] P. W. Stephens, J. Appl. Crystallogr. **27**, 462 (1999).
[35] T. Egami, E. Mamontov, and W. Dmowski, Fund. Phys. of Ferroelectrics **CP677**, 48 (2003).
[36] J. Frantti, J. Lappalainen, S. Eriksson, V. Lantto, S. Nishio, M. Kakihana, S. Ivanov, and H. Rundlöf, Jpn. J. Appl. Phys., Part 1 **39**, 5697 (2000).
[37] L. A. Schmitt, K. A. Schönau, R. Theissmann, H. Fuess, H. Kungl, and M. J. Hoffmann, J. Appl. Phys. **101** 074107 (2007).
[38] R. Schierholz, diploma thesis, Darmstadt University of Technology, 2004; and (private communication).
[39] H. Meštrić, R.-A. Eichel, T. Kloss, K.-P. Dinse, So. Laubach, St. Laubach, P. C. Schmidt, K. A. Schönau, M. Knapp, and H. Ehrenberg, Phys. Rev. B **71**, 134109 (2005).
[40] R.-A. Eichel, H. Meštrić, K.-P. Dinse, A. Ozarowski, J. van Tol, L. C. Brunel, H. Kungl, and M. J. Hoffmann, Magn. Reson. Chem. **43**, S166 (2005).
[41] H. Meštrić, Rüdiger-A. Eichel, K.-P. Dinse, A. Ozarowski, J. van Tol, L. C. Brunel, H. Kungl, M. J. Hoffmann, K. A. Schönau, M. Knapp, and H. Fuess, Phys. Rev. B **73**, 184105 (2006).
[42] H. Meštrić, R.-A. Eichel, K.-P. Dinse, A. Ozarowski, J. van Tol, and L. C. Brunel, J. Appl. Phys. **96**, 7440 (2004).
[43] A. Abragam and B. Bleaney, *Electron Paramagnetic Resonance of Transition Ions* (Clarendon, Oxford, 1970).
[44] V. G. Grachev, Sov. Phys. JETP **65**, 1029 (1987).
[45] Y. Liang, H. Kato, M. Taya, and T. Mori, Scr. Mater. **43**, 535540 (2000).
[46] J. Ricote, R. W. Whatmore, and D. J. Barber, J. Phys.: Condens. Matter **12**, 323 (2000).
[47] L. A. Schmitt, Ph.D. thesis, Darmstadt University of Technology, 2007.
[48] J. Sapriel, Phys. Rev. B **12**, 5128 (1975).
[49] W. L. Warren, B. A. Tuttle, F. C. Rong, G. J. Gerardi, and E. H. Poindexter, J. Am. Chem. Soc. **80**, 680 (1997).
[50] R. G. Pontin, E. F. Slade, and D. J. E. Ingram, J. Phys. C **2**, 1146 (1969).
[51] E. S. Kirkpatrick, K. A. Müller, and R. S. Rubins, Phys. Rev. **135**, A86 (1964).
[52] I. MacLaren, L. A. Schmitt, H. Fuess, H. Kungl, and M. J. Hoffmann, J. Appl. Phys. **97**, 094102 (2005).
[53] M. Leoni, A. F. Gualtieri, and N. Roveri, J. Appl. Crystallogr. **37**, 166 (2004).
[54] L. Bellaiche, A. Garcia, and D. Vanderbilt, Phys. Rev. Lett. **84**, 5427 (2000).
[55] I. Grinberg, V. R. Cooper, and A. M. Rappe, Nature (London) **419**, 909 (2002).
[56] K. Bhattachrya, California Institute of Technology (private communication).
[57] M. Budimir, D. Damjanovic, and N. Setter, Phys. Rev. B **73**, 174106 (2006).
[58] A. J. Bell, J. Mater. Sci. **41**, 13 (2006).
[59] L. Bellaiche, A. Garcia, and D. Vanderbilt, Phys. Rev. B **64**, 060103(R) (2001).